

A ML framework to predict permeability of highly porous media based on PSD

Haoyu Yang^a, Yan Ke^b, Duo Zhang^{c*}

^aDepartment of Chemical Engineering, School of Engineering, University of Edinburgh, EH9 3FB, Edinburgh, United Kingdom

^bDepartment of Engineering, University of Cambridge, Cambridge, CB2 1TN, United Kingdom

^cFaculty of Engineering and Physical Sciences, University of Surrey, Guildford, GU2 7XH, United Kingdom.

*Corresponding email: duo.zhang@surrey.ac.uk

Abstract Using machine learning (ML) method to predict permeability of porous media has shown great potential in recent years. A current problem is the lack of effective models to account for highly porous media with dilated pores. This study includes (1) generation of media (porosity = 0.8) via a Boolean process, (2) the pore size distribution (PSD) control by using different groups of homogeneous packed spherical particles (3) PSD data obtainment using the spherical contact distribution model (4) computation of the permeability via LBM simulations, (4) training of artificial neuron network (ANN) and (5) analysis of the model. It is found that the PSD could outperform the previous geometry descriptors as an input of ML framework to deal with highly porous structures with different fractions of dilated pores, however there is still room for precision enhancement.

1. Introduction

A column filled with packing materials, often denoted as a ‘packed bed’, is ubiquitously applied in many fields of chemical engineering research, especially with separation processes such as absorption and stripping [1]. Due to an escalating demand for designing columns conducting faster separations, the relationship between pressure gradient and the permeability (the rate at which a fluid could flow through the porous media) has been attached with a major significance [2].

Among the orthodox approaches, the models explaining the connection between the matrix characteristics and its capacity for fluid flow were often based on direct experimental data using a core plug method [3, 4]. However, the sample size was constrained by a limitation in resources and time. Previous studies have established several semi-empirical models concerning the permeability based on bed porosity, including the well-known Kozeny-Carman equation (detailed in Ref. [5]). While it remains an intractable question to derive an explicit relationship because of the great complexity and disorder of porous media.

In recent years, several numerical approaches have been proposed to obtain a calculated permeability simply based on 2-D/3-D image-style representation of a structure, such as finite element method (FEM), finite volume method (FVM) and Lattice Boltzmann method (LBM) (detailed in Ref. [6, 7]). FEM and FVM are rigorous simulation methods while fine mesh is essential to guarantee the accuracy of computation results, thus large quantities of computing resources are required in this process [8]. LBM



has been employed more widely thereof at present to simulate fluid flow in porous media due to its superiority of dealing with complex non-regular structures at much lower computing costs [9]. It solves kinetic equations at mesoscopic level where the fluid is discretised as particles while the space as lattice [10]. Although LBM has reduced computing expenses compared with FEM and FVM, it still entails exacting computing environments if direct simulations are carried out [11].

The machine learning (ML) method has been widely utilised in various engineering fields including geoscience, astronomy and biology [12, 13]. This is because ML makes it possible to generate and analyse large volume of data without sophisticated real experiments or demanding computing resources [12]. Instead of anticipating the outputs explicitly, ML algorithms offer an alternative way recognised as far easier; to train a system by showing it examples of desired output-input pairs [13].

And a specific aspect; the neural network algorithms have drawn great attention for it could give convincing results in data classification [14]. Convolutional neural networks (CNN) and traditional artificial neural networks (ANN) have both shown prominent performance in some relevant geoscience researches to predict physical properties of porous rock, which would be illuminating to our study since permeability could be solely expressed by functions of geometry parameters [15-17]. Lähivaara et al. [15] presented a CNN model predicting porosity and tortuosity based on images gathered by ultrasound tomography technology. And the preliminary study of Srisutthiyakorn [16] elucidated the promising future of predicting permeability using ANN or CNN algorithms combined with LBM from 2-D or 3-D images.

There have been some attempts to predict permeability from images [17] or extracted information [18] in more recent studies. And the feasibility of predicting permeability using combined ML and LBM has been validated. Wu et al. [17] proposed a physics-informed CNN model incorporating the variables porosity and specific surface area into the network architecture. The inputs were both 2-D images and the two chosen geometric properties of porous media and the network was trained with results from a D2Q9 LBM model. This modified network proved to have a better performance than conventional CNN models. However, this model could become computational expensive as complicated structures can lead to large input dimensions. The up to date work by Tian et al. [18] intended to provide a more comprehensive understanding concerning this issue. An ANN network based on extracted features was used to reduce the input size. 15 physical features including global properties, pore information and throat information were taken into account. These parameters were extracted by pore network model (PNM) from 3-D structures. This network was trained with results from a D3Q19 LBM model. This framework was extremely reliable for structures with low porosities (0.1 and 0.3), while large porosities were not tested.

Despite these previous works have developed some precious insights into the permeability predicting problem, it remains an issue that the current predictive models perform unsatisfactorily when processing structures with large porosities and dilated pores [17]. Therefore, it is of interests to select new suitable geometry descriptors as input variables [19]. To find a promising solution, the pore size distribution (PSD) has been recognised as an alternative descriptor instead of the preceding extracted features. The PSD had been attached with great importance decades earlier [20, 21]. Also there have been some semi-empirical simulations investigating the influence of pore size on the permeability of a system in recent years [22-25]. Promisingly it could be a potential substitute for complicated matrix properties but to the best of our knowledge there has not been model predicting the permeability from the PSD, nevertheless. Compared with the previous model, we extract the statistical PSD data of the whole system which could cover the pore information mentioned in Ref. [17, 18] and give more detailed geometric information about the system.

In our study, we construct an ANN framework to predict permeability based on PSD data. In section 2, the porous media are generated with the same porosity (0.8) through a Boolean process. Homogeneous circles are inserted into a 2-D square to simulate the training porous media. A Wide range of PSD is realised by adjusting the radius of the scattered circles when generating different media. In the test sets, homogeneous and heterogeneous generations are both considered to test the universality of the model. Then in Section 3, the permeabilities of the structures are calculated using LBM and the simulation

results are regarded as true permeability values. Section 4 has described both the classification and the regression model used in this result, with the results shown in section 5. The prediction results demonstrate that, the PSD data could be a qualified input to give fast and acceptable predictions, especially for structures of high porosity and dilated pores.

2. Porous media processing

2.1. Porous media generation

The generation of 2-D artificial media could be realised through a Boolean process [26]. A typical Boolean process consists of two steps. Firstly, points x_i (called germs) are scattered stochastically and independently across the domain. Secondly, a random object Z_i (called a grain) is placed at every point x_i . Then the output of the Boolean process Z could be calculated as the union set of all such germ-grain pairs. Such pairs are to simulate the solid components within the matrix.

$$Z = \bigcup_{i=1}^n (Z_i + x_i) \quad (1)$$

In our study, the process was operated in a $300 \times 300 \text{ lu}^2$ (lu : lattice unit) square and the random objects (grains) were set to be circles with identical radii. The porosity equalled the quotient of the number of lattices not occupied with germ-grain pairs to the total number of lattices, i.e., 90000. To control the porosity, the number of germ-grain pairs was not predefined. Instead, they were inserted until the given porosity ϕ is achieved. In the current paper, the porosity was set to be 0.8.

In order to guarantee a relatively wide PSD range, the overall generation process was divided into five groups according to the radii of the randomly packed particles ($r = 10, 15, 20, 25, 30$). In our study, the boundary condition was determined as the periodic condition (detailed in Ref. [7]), i.e., if a circle reached one edge of the square, the excess part shifted to the other side.

Samples of porous structures obtained were shown in **Figure. 1**.

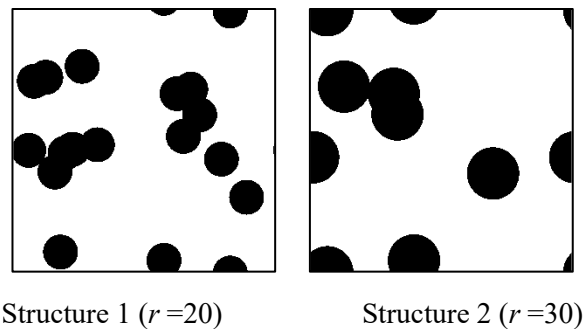


Figure. 1. Porous media generated by a Boolean Process

2.2. Porosity rectification

The procedure above provided 2-D porous media figures with close porosity values. While the open porosity ϕ_0 is distinguished from the porosity ϕ [26]. The open porosity was calculated only based on the conducting phase, thus in this process the sealed cavities were filled with the solid phase. The recalculated open porosity ϕ_0 could describe the fraction of actual conducting pore space of a medium. Given that the open porosity could be lower than the predetermined value, the deviation was controlled at a level of 0.5%. Qualified media were selected for the subsequent operations. The structure transformation was illustrated as below (**Figure. 2**).

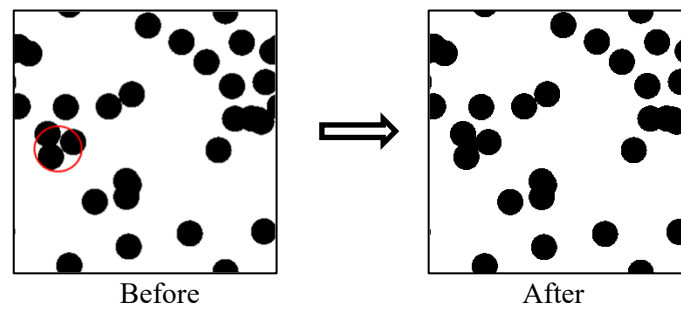


Figure 2. The closed cavity filling process

After this process, we obtained 400 structures for each radius group, i.e., 2000 structures in total. Then the order of the structures was rearranged randomly, 1800 of which were put into the training set, and the rest 200 were assigned to test set 1. To further examine the predictive precision, another 200 structures generated with varied radii (ranged from 10 to 30) were selected as test set 2.

2.3. PSD acquisition

The pore size distribution could be represented with the spherical contact distribution [27, 28]. This process was realised by inserting a circle at every pore lattice, the diameter of which was increased until it first encountered a solid lattice. Then the discrete pore size of each pore lattice was defined as the largest diameter of such circles that could include the lattice. Finally, the obtained pore sizes were categorised into 10 evenly spaced groups with respect to the diameter values, from 20 to 200 lattice units respectively. The pore size distribution of 2 sample media with the same porosity were given in **Figure 3**.

It is overtly shown that different media would have different PSD data. Generally, structures generated with larger circles are prone to have more large pores. The pore size could demonstrate the distance of each lattice to the nearest solid phase and the pore throat information is also embodied in this process by considering the small pores in the structure. Besides this PSD extraction method could provide relatively larger dataset which could cover all points inside a medium compared with former works [17, 18]. And with this approach, we successfully reduce the input dimensionality to a simple 10×1 matrix, which could be computed less than 20 seconds for a single figure. Also, it enables us to apply fast ML network in the subsequent predicting process.

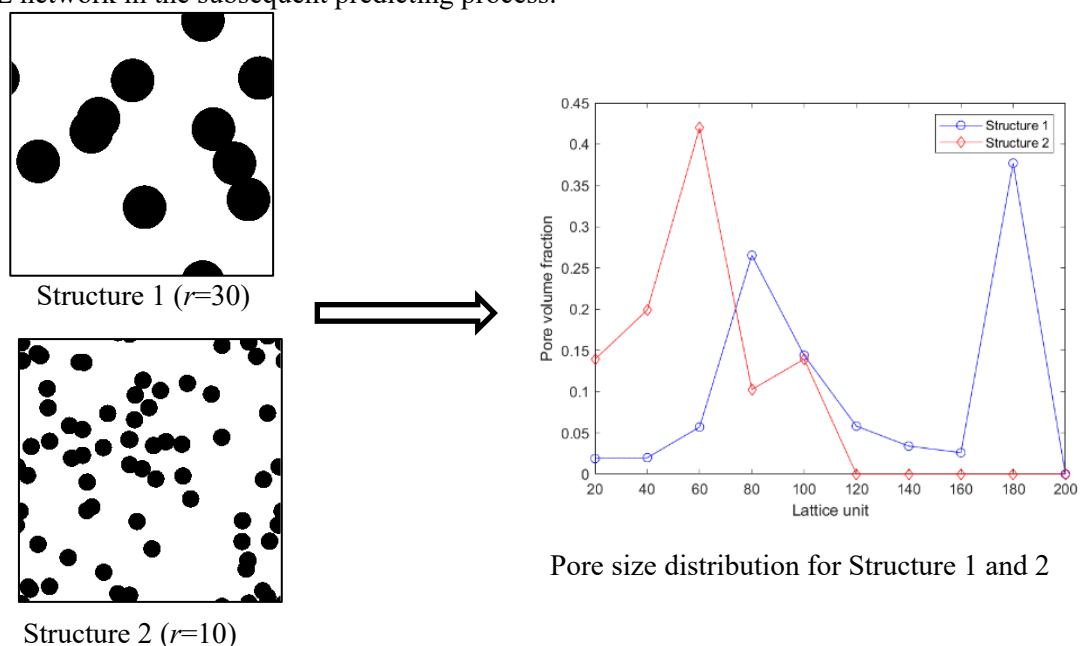


Figure 3. The pore size distribution of sample media

3. Permeability calculation based on LBM

In this article, the LBM was applied to calculate the permeability of the 2-D porous media obtained in the previous section. In this paper, the D2Q9 model mentioned in Ref. [7] was used for lattice arrangements, as illustrated in **Figure 4** [7].

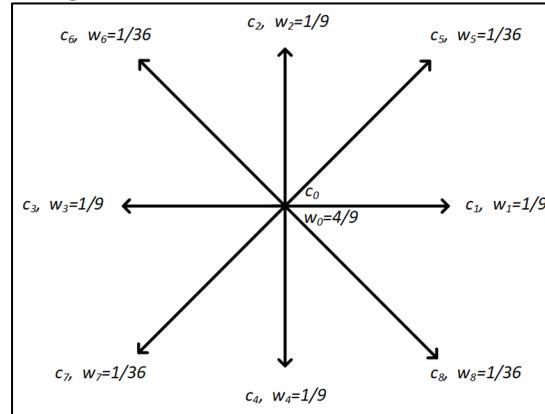


Figure 4. D2Q9 model for velocity discretisation

And we used the single-relaxation-time lattice Boltzmann (BGK) model in the current paper, which could be written as:

$$f_i(\mathbf{x} + \mathbf{e}_i \delta_t, t + \delta_t) - f_i(\mathbf{x}, t) = -\frac{[f_i(\mathbf{x}, t) - f_i^{eq}(\mathbf{x}, t)]}{\tau} + \mathbf{F}_i \quad (2)$$

Where:

f_i – The particle distribution along i direction;

f_i^{eq} – The equilibrium distribution;

δ_t – Time step;

\mathbf{e}_i – The particle velocity in i direction;

τ – The single relaxation time;

\mathbf{F}_i – The body force term;

The velocity vector in all 9 directions is defined by:

$$\mathbf{e} = c \begin{bmatrix} 0 & 1 & 0 & -1 & 0 & 1 & -1 & -1 & 1 \\ 0 & 0 & 1 & 0 & -1 & 1 & 1 & -1 & -1 \end{bmatrix} \quad (3)$$

Where:

c – The lattice speed, $c = \delta_x / \delta_t$ and δ_x is the lattice spacing;

The equilibrium distribution function f_i^{eq} is calculated as:

$$f_i^{eq} = \rho w_i \left[1 + \frac{\mathbf{e}_i \cdot \mathbf{v}}{c_s^2} + \frac{(\mathbf{e}_i \cdot \mathbf{v})^2}{2c_s^4} - \frac{\mathbf{v} \cdot \mathbf{v}}{2c_s^2} \right] \quad (4)$$

$$w_i = \begin{cases} \frac{4}{9} & i = 0; \\ \frac{1}{9} & i = 1, 2, 3, 4; \\ \frac{1}{36} & i = 5, 6, 7, 8; \end{cases} \quad (5)$$

Where:

\mathbf{v} – The velocity;

c_s – The lattice sound speed, $c_s = c / \sqrt{3}$;

w_i – The weight of discrete velocities;

The force term F_i is given by:

$$F_i = \left(1 - \frac{1}{2\tau}\right) w_i \left[\frac{\mathbf{e}_i - \mathbf{v}}{c_s^2} + \frac{\mathbf{e}_i \cdot \mathbf{v}}{2c_s^4} \mathbf{e}_i \right] \cdot \mathbf{F} \quad (6)$$

The macroscopic density and momentum could be obtained as following summations:

$$\rho = \sum_{i=0}^8 f_i \quad (7)$$

$$\rho \mathbf{v} = \sum_{i=0}^8 f_i \mathbf{e}_i + \frac{\mathbf{F}}{2} \quad (8)$$

The settings of the LBM simulations are shown in **Table 1**.

Table 1. Settings of LBM simulations

Model	Lattice unit	Boundary condition	Body force	Relaxation time	Density	Steady state condition
D2Q9-SRT	300	Periodic	0.01	0.6	1000	Relative error (consecutive steps) $< 10^{-8}$

4. Framework of permeability predicting

In this study, ANN was used to predict the permeability. The basis of ANNs is inspired by the nervous system of the human brain. A neuron is a fundamental computation unit with several inputs and one output [29]. A layer is constructed by neurons, and the neurons of adjacent layers are connected to each other by weights. A typical ANN would consist of three types of layers, namely the input, hidden and output layer. Within a neuron, the output is calculated by the activation function f which could be expressed as follows:

$$y_j = f \left(\sum_{i=1}^n w_{ij} x_i + b \right) \quad (9)$$

Where:

w_{ij} – The weight between i th neuron (from the previous layer) and j th neuron (from the current layer);

x_i – The output from i th neuron;

y_j – The output of j th neuron;

b – The constant bias term;

A single neuron and a conventional multi-layer ANN are illustrated in **Figure 5** [18].

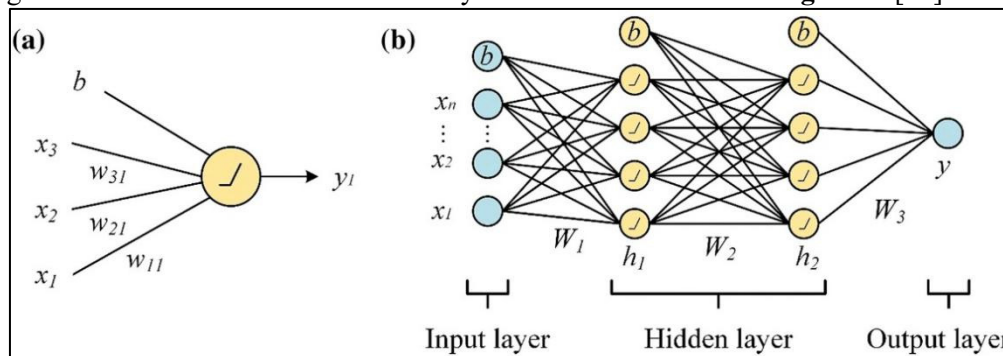


Figure 5. ANN illustration: (a) single neuron and (b) multilayer structure [18]

To verify the feasibility of permeability prediction using PSD data, this research used both a classification model and a regression model. As mentioned in Section 2, the input was set as a 10×1 matrix which enabled a relatively simple network structure, thus reducing the processing time.

4.1. Classification prediction

Firstly, the permeability of media was split into 3 categories. The range of each group was defined to have roughly equal size to avoid a ‘preference’ in classification, i.e., to prohibit the model from heavily biasing towards one group because most of the training data fell into the same section. The permeability of the training set was plotted versus each sample in **Figure 6**.

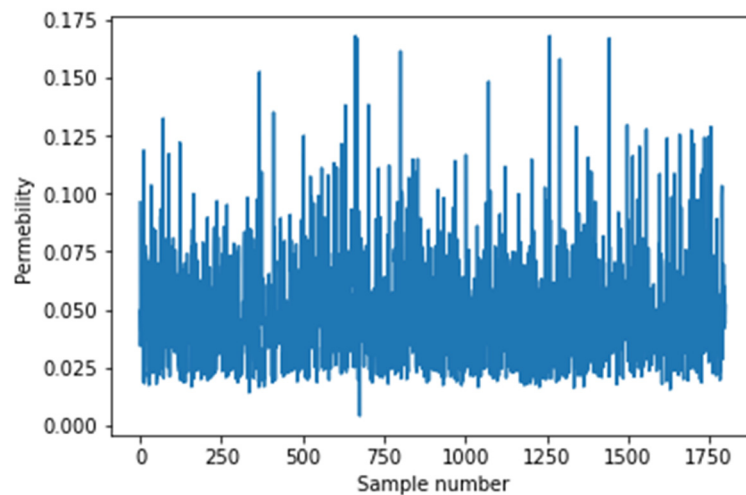


Figure 6. Permeability on the training set

After calculation, the permeability range was decided as low (< 0.036), medium (0.036 to 0.054) and high (> 0.054), respectively. And the numbers of structures in each group were shown in **Table 2**.

Table 2. Permeability division

	Low (< 0.036)	Medium (0.036 to 0.054)	High (> 0.054)
Number	599	614	587

For this classification problem, we used only one hidden layer which contained 10 neurons and was activated with the rectified linear unit (ReLU) function. And the smooth argmax (Softmax) function was used in the output layer to identify the category with the highest probability. In this classifier, the final output permeability labels were expressed with natural numbers; 0, 1, and 2 for low, medium and high severally.

4.2. Regression prediction

A regression algorithm was also developed. The same dataset was used to train the network. However, the label of the regressor is permeability instead of the categories used in the classification model. For the regression problem, two hidden layers with 10 neurons each were constructed. The ReLU function was applied to activate both layers. The output layer simply consisted of a value given by the regressor.

5. Result and discussion

5.1. Classification prediction

The predictive model is preliminarily assessed by the classification accuracy. In this 3-group classification case, the results are shown in **Table 3**. And the mean deviations are shown in **Table 4**.

Here the prediction deviation is defined as the absolute difference between the predicted label and the test label.

Table 3. Classification accuracy

	Training set	Test set 1	Test set 2
Accuracy	0.7389	0.7900	0.6750

Table 4. Prediction deviations

	Test set 1	Test set 2
Deviation = 0	n = 158	n = 135
Deviation = 1	n = 41	n = 62
Deviation = 2	n = 1	n = 3
Mean Deviation	0.215	0.340

Both test sets show acceptable accuracies which are much higher than a random prediction (33%). The feasibility of this predictive model based on PSD data is therefore validated and the overfitting problem is avoided. The predictive performance on test set 1 could surpass that on test set 2, which could be concluded from both the accuracy and the mean deviation. This is rational because structures of the training set and set 1 are generated with homogeneous particles while those of test set 2 are formed by heterogeneous particles.

While it is undesirable that the accuracy on test set 1 is even better than the training set, which would indicate that the classifier is weak. It is reasonable because the performance of a classification predictive model could not be merely evaluated by the accuracy when it is used to predict a continuous variable. The model could only be applied in a rough screening test; the permeability is discretised when there are no strict precision requirements. To further examine the exactitude of PSD data as a geometry descriptor, a regression model is applied.

5.2. Regression prediction

The predicted and test permeabilities are shown in **Figure 7**.

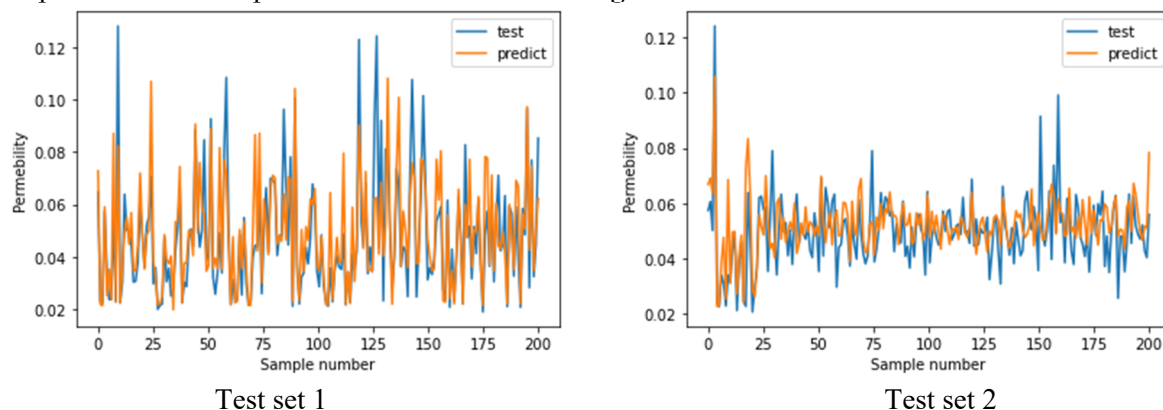


Figure 7. Comparison between predicted and test permeability

R^2 scores and mean squared errors (MSE) are calculated to provide a quantitative analysis of the prediction. The definitions are expressed as follow:

$$R^2 = 1 - \frac{\sum_{i=1}^n (k_{i,ANN} - k_{i,LBM})^2}{\sum_{i=1}^n (k_{i,LBM} - \bar{k}_{LBM})^2} \quad (10)$$

$$MSE = \frac{1}{n} \sum_{i=1}^n (k_{i,ANN} - k_{i,LBM})^2 \quad (11)$$

The results are shown in **Table 5**.

Table 5. R^2 scores and MSE of test sets

	R^2 score	MSE
Test set 1	0.60961	0.00019
Test set 2	0.17355	0.00016

Besides, in practical applications, the relative errors are always of interests when assessing a model. The cumulative frequency curves for relative errors of both sets are shown in **Figure 8** to give a general overview of the case.

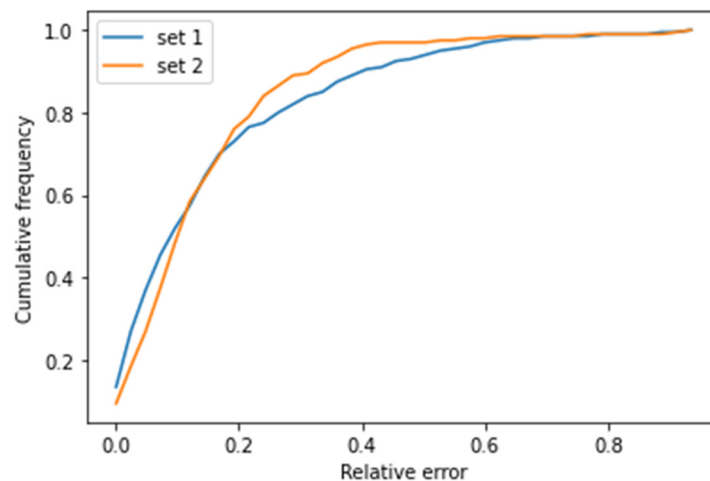


Figure 8. Cumulative frequency curves of two test sets

According to the definition of R^2 , roughly 61% of the variation observed on test set 1 could be explained by the input PSD data while on test set 2 the proportion decreases to 17%. Compared with experimental R^2 scores obtained by the previous work, the result on test set 1 (0.60961) proves much better than results given by the Kozeny-Carman equation (-65.15538), the conventional CNN (-0.71426) and the modified CNN proposed by Wu et al (0.20495) [17]. R^2 score on test set 2 (0.17355) implies that our ANN still provides more convincing results than the first two models in more general (heterogeneous) cases.

The MSE is another criterion which measure the quality of a regressor. Although there is a contrast between R^2 scores, the MSEs of the two sets are relatively close. This could suggest that the oscillations in test set 2 are rather moderate compared to test set 1, i.e., the data distribution is more concentrated. This could also be deduced from **Figure 7**. The similarity in permeabilities could be explained by the generation procedure of test set 2; the structures are generated with heterogeneous particles but from the same set (radii ranged from 10 to 30), so the morphology of media would be identical statistically (detailed described by Minkowski functionals in Ref. [30]).

Based on the aforementioned results, it is shown that the current regression predictive model could not give precise predictions on minor permeability variations in semblable structures while it proves

better performance on test structures generated with larger morphological differences. However, the majority of predicted values have less than 20% error compared with the simulated ones, so it could still be adapted when there is no rigorous limit on relative errors.

5.3. Future outlook

Because this framework is relatively primitive at present, a much better performance could be expected if further modifications are made. Some common methods including using more extracted features as inputs or applying other algorithms to tune the network could be adopted.

Other more specific approaches for this case could also be considered. One of the major limitations in the current study is that the model is not 'acute' enough when dealing with similar structures. The possible solutions will focus on how to describe the structures more elaborately. From this point we could reduce the size intervals when obtaining the PSD data, or we could use more homogeneous groups when generating the training media.

In conclusion, using the PSD as a geometry descriptor to predict permeability could be potentially more effective than some previous inputs, especially for structures of high porosity. More attempts could be made in this aspect to examine the performance of this model in practical applications.

6. Conclusion

In this paper, an ANN is proposed to discover the implicit relationship between permeability and the PSD data. The research includes several procedures: (1) generating porous media with the same porosity (0.8) via a Boolean process, (2) obtaining PSD data using the spherical contact distribution model (3) obtaining permeabilities applying LBM simulations, (4) training ANN and (5) applying the trained network to predict permeabilities of new structures in the test sets. The model overperforms some previous models when it is used to predict media of a large porosity and with various fractions of dilated pores. The relative errors between most predictions and the corresponding simulations are less than 20%. The model verifies the operability of using PSD as the input geometry descriptor particularly when dilated pores exist. The ANN permeability prediction method should be orders of magnitude faster than direct simulation, and using PSD as inputs also significantly reduces computational time compared to models based on images or plenty of other features. Thus, the framework would have promising future in engineering fields.

References

- [1] Seader, J.D. & Henley, Ernest J. (2006). *Separation Process Principles* (2nd edition.). John Wiley & Sonstahm. [ISBN 0-471-46480-5](#).
- [2] H. M. Quinn and J. J. Takarewski, "High performance liquid chromatography method and apparatus," US Patent no. 5,772,874, 1998.
- [3] D. C. Hughes, & R. Amtsbüchler. (1986). Pore Structure and permeability of hardened cement paste*. *Magazine of Concrete Research*, 38(137), 230-231.
- [4] Bágel', L., & Živica, V. (1997). Relationship between pore structure and permeability of hardened cement mortars: On the choice of effective pore structure parameter. *Cement and Concrete Research*, 27(8), 1225-1235.
- [5] Quinn, H. (2014). A Reconciliation of Packed Column Permeability Data: Column Permeability as a Function of Particle Porosity. *Journal of Materials*, 2014, 1-22.
- [6] Versteeg, H., & Malalasekera, W. (2007). *An introduction to computational fluid dynamics the finite volume method* (2nd edition). Harlow, Essex: Pearson Education.
- [7] Mohamad, A. (2011). *Lattice Boltzmann method fundamentals and engineering applications with computer codes*. London; New York: Springer.
- [8] Borujeni, A., Lane, N., Thompson, K., & Tyagi, M. (2013). Effects of image resolution and numerical resolution on computed permeability of consolidated packing using LB and FEM pore-scale simulations. *Computers & Fluids*, 88(C), 753-763

- [9] Hao, L., & Cheng, P. (2010). Pore-scale simulations on relative permeabilities of porous media by lattice Boltzmann method. *International Journal of Heat and Mass Transfer*, 53(9), 1908-1913.
- [10] Chen S, Doolen GD (1998) Lattice Boltzmann method for fluid flows. *Annual Review of Fluid Mechanics*, 30(1), 329–364.
- [11] Blunt, M., Bijeljic, B., Dong, H., Gharbi, O., Iglauer, S., Mostaghimi, P., Pentland, C. (2013). Pore-scale imaging and modelling. *Advances in Water Resources*, 51, 197-216.
- [12] Al-Jarrah, O., Yoo, P., Muhaidat, S., Karagiannidis, G., & Taha, K. (2015). Efficient Machine Learning for Big Data: A Review. *Big Data Research*, 2(3), 87-93.
- [13] Jordan MI, Mitchell TM. (2015). Machine learning: trends, perspectives, and prospects. *Science* 349(6245), 255–260
- [14] Lecun, Y., Bengio Y., & Hinton G. (2015). Deep Learning. *Nature*, 521(7553), 436.
- [15] Lähivaara, T., Kärkkäinen, L., Huttunen, J., & Hesthaven, J. (2018). Deep convolutional neural networks for estimating porous material parameters with ultrasound tomography. *The Journal of the Acoustical Society of America*, 143(2), 1148-1158.
- [16] Srisutthiyakorn, N. (2016). Deep-learning methods for predicting permeability from 2D/3D binary-segmented images. *2016 SEG International Exposition and Annual Meeting*, 2016 SEG International Exposition and Annual Meeting, 2016.
- [17] Wu, J., Yin, X., & Xiao, H. (2018). Seeing permeability from images: Fast prediction with convolutional neural networks. *Science Bulletin*, 63(18), 1215-1222.
- [18] Tian, J., Qi, C., Sun, Y., Yaseen, Z., & Pham, B. (2020). Permeability prediction of porous media using a combination of computational fluid dynamics and hybrid machine learning methods. *Engineering with Computers*.
- [19] Jablonka, Kevin Maik, Ongari, Daniele, Moosavi, Seyed Mohamad, & Smit, Berend. (2020). Big-Data Science in Porous Materials: Materials Genomics and Machine Learning. *Chemical Reviews*, 120(16), 8066-8129.
- [20] T. J. Marshall. (1958). Permeability and the Size Distribution of Pores. *Nature*, 181(4607), 477.
- [21] Childs, E., & Collis-George, N. (1950). The Permeability of Porous Materials. *Proceedings of the Royal Society of London. Series A, Mathematical and Physical Sciences (1934-1990)*, 201(1066), 392-405.
- [22] Minagawa, H., Sakamoto, Y., Komai, T., Narita, H., Mizutani, K., Ohga, K., Yamaguchi, T. (2009). Relation between Pore-size Distribution and Permeability of Sediment. *The Nineteenth International Offshore and Polar Engineering Conference*, the Nineteenth International Offshore and Polar Engineering Conference, 2009.
- [23] Yuan, Y., Gholizadeh Doonechaly, N., & Rahman, S. (2016). An Analytical Model of Apparent Gas Permeability for Tight Porous Media. *Transport in Porous Media*, 111(1), 193-214.
- [24] Geng, L., Li, G., Tian, S., Sheng, M., Ren, W., & Zitha, P. (2017). A fractal model for real gas transport in porous shale. *AIChE Journal*, 63(4), 1430-1440.
- [25] Tian, S., Ren, W., Li, G., Yang, R., & Wang, T. (2017). A Theoretical Analysis of Pore Size Distribution Effects on Shale Apparent Permeability. *Geofluids*, 2017, 9.
- [26] Scholz, Christian, Wirner, Frank, Götz, Jan, Rüde, Ulrich, Schröder-Turk, Gerd E, Mecke, Klaus, & Bechinger, Clemens. (2012). Permeability of porous materials determined from the Euler characteristic. *Physical Review Letters*, 109(26), 264504.
- [27] Zhang, D., Papadakis, K., & Gu, S. (2016). A lattice Boltzmann study on the impact of the geometrical properties of porous media on the steady state relative permeabilities on two-phase immiscible flows. *Advances in Water Resources*, 95(C), 61-79.
- [28] Stoyan, D., Chiu, S., Kendall, W., & Mecke, J. (2013). *Stochastic geometry and its applications*. (Third edition / Sung Nok Chiu, Dietrich Stoyan, Wilfrid S. Kendall, Joseph Mecke.. ed., Wiley series in probability and statistics). Chichester, West Sussex, United Kingdom: John Wiley & Sons.

- [29] McCulloch, W, & Pitts, W. (1990). A logical calculus of the ideas immanent in nervous activity. *Bulletin of Mathematical Biology*, 52(1-2), 99-115.
- [30] Mecke, K. (1997). Morphology of spatial patterns - Porous media, spinodal decomposition and dissipative structures. *Acta Physica Polonica B*, 28(8), 1747-1782.